ACS Infectious Diseases

Letter

Cite This: ACS Infect. Dis. 2020, 6, 56−63

pubs.acs.org/journal/aidcbc

Large-Scale Chemical-Genetic Strategy Enables the Design of Antimicrobial Combination Chemotherapy in *Mycobacteria*

Eachan O. Johnson,[†,‡,§] Emma Office,[†] Tomohiko Kawate,[†,‡,§] Marek Orzechowski,[†] and Deborah T. Hung*[,†,‡,§]

[†]Broad Institute of MIT and Harvard, 415 Main Street, Cambridge, Massachusetts 02142, United States

[‡]Department of Molecular Biology and Center for Computational and Integrative Biology, Massachusetts General Hospital, 185 Cambridge Street, Boston, Massachusetts 02114, United States

[§]Department of Genetics, Harvard Medical School, 77 Avenue Louis Pasteur, Boston, Massachusetts 02115, United States

Supporting Information

ABSTRACT: The efficacies of all antibiotics against tuberculosis are eventually eroded by resistance. New strategies to discover drugs or drug combinations with higher barriers to resistance are needed. Previously, we reported the application of a large-scale chemical-genetic interaction screening strategy called PROSPECT (PRimary screening Of Strains to Prioritize Expanded Chemistry and Targets) for the discovery of new *Mycobacterium tuberculosis* inhibitors, which resulted in the identification of the small molecule BRD-8000, an inhibitor of a novel target, EfpA [Johnson et al. (2019) *Nature 517*, 72]. Leveraging the chemical genetic interaction profile of BRD-8000, we identified BRD-9327, another structurally distinct small molecule EfpA inhibitor. We show that the two compounds are synergistic and display collateral sensitivity because of their distinct modes of action and resistance mechanisms. High-level resistance to one increases the sensitivity to and reduces the emergence of resistance to the other. Thus, the combination of BRD-9327 and BRD-8000 represents a proof-of-concept for the novel strategy of leveraging chemical genetics in the design of antimicrobial combination chemotherapy in which mutual collateral sensitivity is exploited.

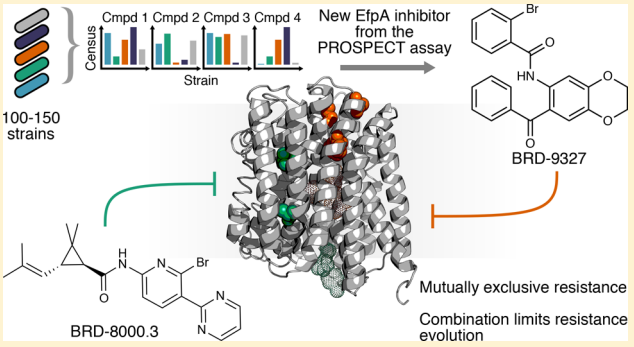

KEYWORDS: *antimicrobial resistance, tuberculosis, chemical genetics, drug discovery, collateral sensitivity, synergy*

Diseases caused by mycobacteria are a significant public health burden, with *Mycobacterium tuberculosis* (Mtb) in particular causing >1.6 million deaths from tuberculosis (TB) annually.[1] The standard of care for drug-susceptible TB is a six-month regimen based on rifampin, isoniazid, pyrazinamide, and ethambutol, but an increasing incidence of multidrug resistant (MDR) TB[1] is forcing the deployment of less effective but longer, more expensive, and more toxic regimens, although improved regimens are in development.[2] With antimycobacterial discovery and development struggling to fill the gaps created by emerging resistance, there is an unmet need for new drugs against TB.

New strategies to discover drugs or drug combinations with higher barriers to resistance are needed. While combination therapy has been the major underlying principle to evade resistance evolution, informed decisions on the best combinations, taking into account the interactions of individual compounds and their resistance mechanisms, has to date been lacking. Here, we propose leveraging large-scale chemical interaction studies to identify compound sets that inhibit the same target, thereby enabling the discovery of pairs of compounds that exhibit collateral sensitivity. Collateral sensitivity, which is resistance to a compound that confers hypersensitivity to another, results in a combination whose resistance barrier is higher than two noninteracting compounds.

Previously, we reported a sequencing-based, large-scale chemical-genetic screening strategy, PRimary screening Of Strains to Prioritize Expanded Chemistry and Targets (PROSPECT), which generated chemical genetic interaction profiles (CGIPs) that characterized the fitness of 150 multiplexed, genetically barcoded hypomorph mutants (strains depleted of individual essential gene products) of Mtb H37Rv in response to ∼50 000 compounds (Figure 1A).[3] PROSPECT quantifies the fitness changes of genetically barcoded hypomorph strains on compound treatment; the vector of fitness changes, measured as log(fold-change) of the abundance of barcodes of a particular hypomorph after treatment with a compound of interest relative to a vehicle control, is known as a CGIP (Figure 1A). Addressing the need for MOA diversity in tackling antimicrobial resistance,

Received: September 27, 2019
Published: November 13, 2019

DOI: 10.1021/acsinfecdis.9b00373
ACS Infect. Dis. 2020, 6, 56−63

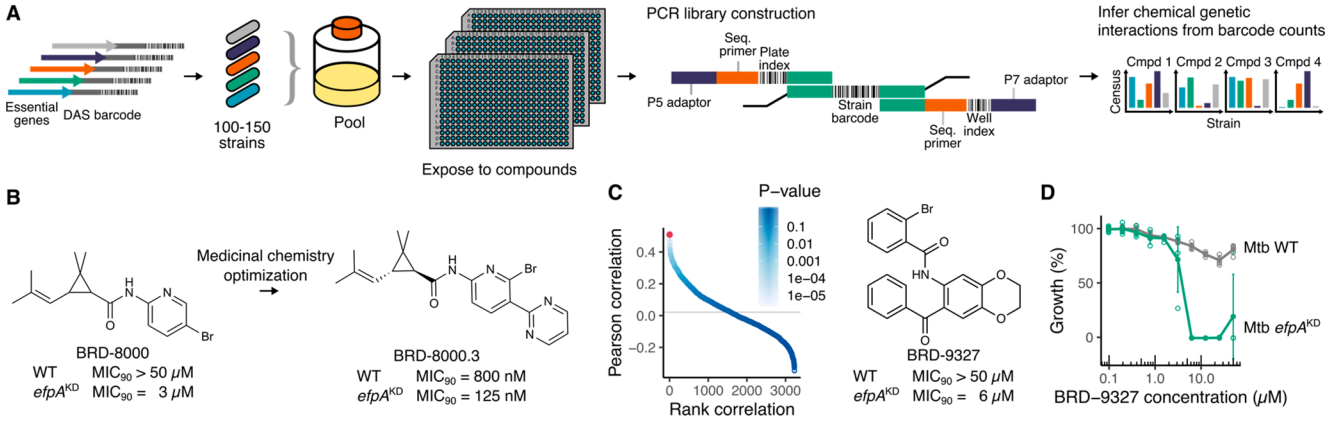

Figure 1. Discovery of a new putative inhibitor of the essential mycobacterial efflux pump, EfpA. (A) Overview of PROSPECT, a sequencing-based, high-throughput chemical-genetic profiling assay. A C-terminal DAS tag, which targets the gene product to degradation by caseinolytic protease (Clp), was integrated at the 3′ end of target genes of interest in the chromosome with concomitant genetic barcoding, which allowed pooling of hypomorph strains. After compound exposure, chromosomal barcodes were PCR amplified, sequenced on the Illumina platform, and analyzed for changes in abundance relative to vehicle controls. For each compound, this generated a vector of strain abundance changes, known as a chemical genetic interaction profile (CGIP). (B) Medicinal chemistry optimization of initial hit BRD-8000, an EfpA inhibitor, yielded BRD-8000.3, a narrow-spectrum antimycobacterial with good wild-type activity. (C) Ranked Pearson correlation of CGIPs with the BRD-8000 CGIP. Each point represents a compound's CGIP correlation; blue shading indicates the *P*-value under a permutation test (n = 10 000). Since BRD-8000 had been validated as an EfpA inhibitor, its CGIP could be used as a reference to discover further EfpA inhibitors. The CGIP of BRD-9327 (highlighted in red) had the highest correlation with the CGIP of BRD-8000. (D) Broth microdilution assay of BRD-9327 against wild-type Mtb and its EfpA hypomorph (Mtb $efpA^{KD}$); open circles show individual replicates (n = 4), filled circles indicate the mean, and error bars show the 95% confidence interval. BRD-9327 showed very little activity against wild-type Mtb, although the EfpA hypomorph was hypersensitive.

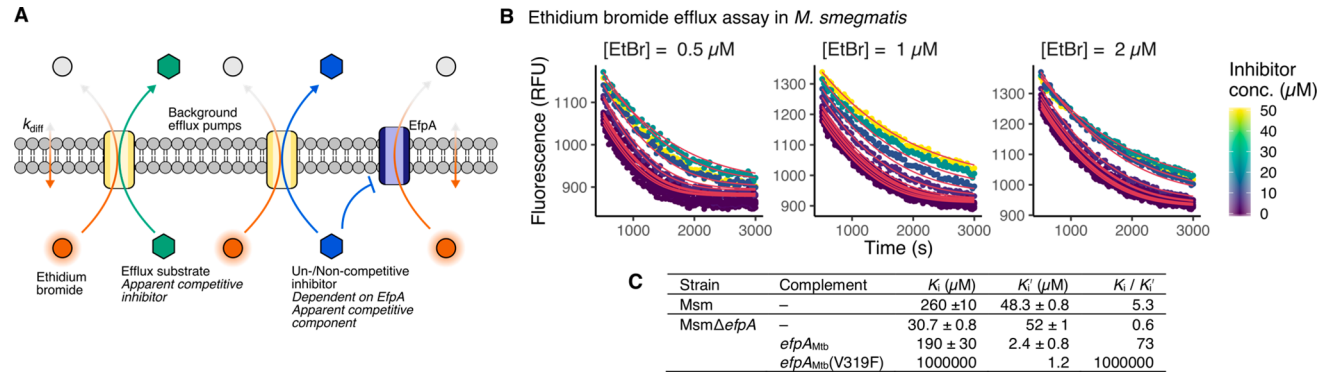

Figure 2. Validating EfpA as the target of BRD-9327 using an EtBr efflux assay. (A) Overview of molecular basis of the EtBr assay for determining kinetic inhibition parameters. When intracellular, EtBr (orange) is ~30-fold more fluorescent than extracellular; thus, EtBr fluorescence is a proxy for intracellular concentration. In living cells, a compound, which is simply a substrate of efflux pumps (green hexagon), will exhibit a competitive mode of EtBr efflux inhibition, since it competes with EtBr for flux through the pumps. However, a compound that has a specific interaction with EfpA (blue hexagon) might also appear to inhibit EtBr efflux competitively but will exhibit an additional non- or uncompetitive modality. In the absence of EfpA, as in a null mutant, this non- or uncompetitive modality will be abolished. (B) EtBr fluorescence decay over time (demonstrating varying efflux rates) at three starting intracellular concentrations and eight BRD-9327 concentrations in Msm. Curves corresponding to global best-fit Michaelis–Menten parameter estimates are shown in red. (C) Global best-fit Michaelis–Menten parameter estimates (±standard deviation) of EtBr efflux inhibition by BRD-9327.

PROSPECT can be used to prioritize compounds from primary phenotypic screening data based on their putative MOA, instead of simply their potency. We illustrated PROSPECT's strengths in the discovery of BRD-8000, an uncompetitive inhibitor of a novel target, EfpA (Rv2846c), an essential efflux pump in Mtb. Though BRD-8000 itself lacked potent activity against wild-type Mtb (minimal inhibitory concentration, MIC ≥ 50 μM), chemical optimization yielded BRD-8000.3, a narrow-spectrum, bactericidal antimycobacterial agent with good wild-type activity (Mtb MIC = 800 nM, Figure 1B).[3]

A fundamental strength of PROSPECT is its generation of a large panel of chemical-genetic interactions (7.5 million in the previously reported screen[3]) that can be iteratively and retrospectively mined for new interactions of interest. For example, upon validation of a new a novel inhibitor's mechanism of action (MOA), its CGIP can be used as a reference for the subsequent discovery of additional scaffolds that work by inhibiting the same target. Taking this approach, we used the CGIP of BRD-8000 to retrospectively identify and prioritize additional putative EfpA inhibitors from the same primary screening data based on their CGIP correlation with BRD-8000s CGIP (Figure 1C). The chemically distinct molecule BRD-9327 emerged as another possible EfpA inhibitor.

DOI: 10.1021/acsinfecdis.9b00373
ACS Infect. Dis. 2020, 6, 56–63

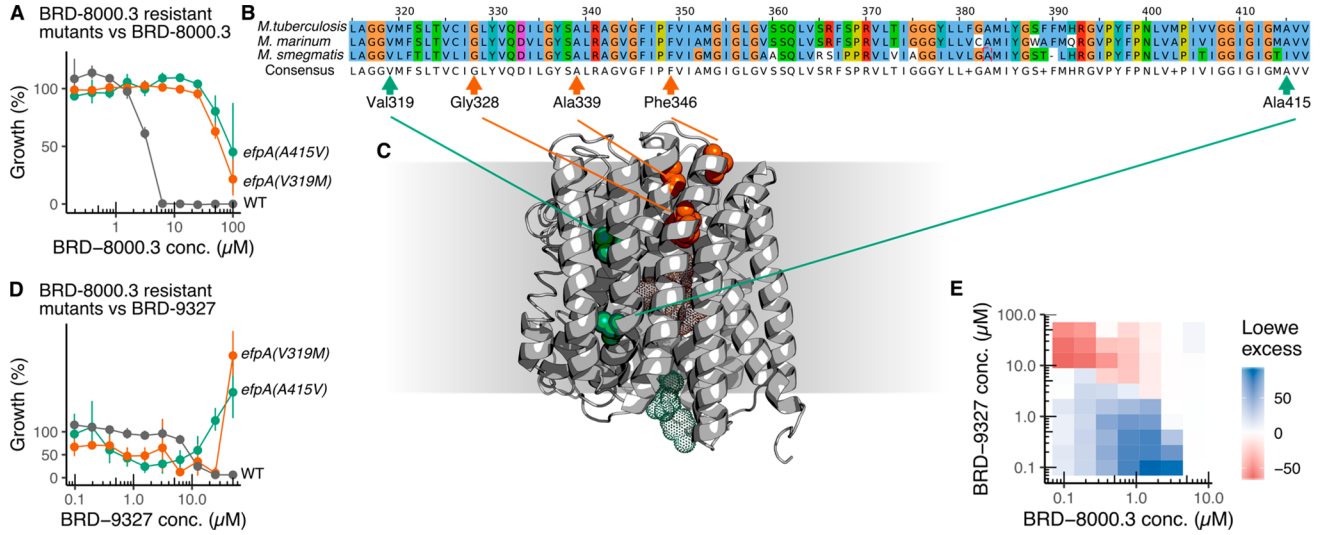

Figure 3. Evolution of Mmar mutants resistant to BRD-8000.3 or BRD-9327. (A) Broth microdilution dose response assay of Mmar and its BRD-8000.3-resistant mutants against BRD-8000.3, demonstrating their high-level resistance to this compound. Filled circles show the mean, and error bars indicate the 95% confidence interval (n = 4). (B) Amino acid sequence alignment of highly conserved EfpA in Mtb, Mmar, and Msm, with sites conferring resistance to BRD-8000.3 (green) or BRD-9327 (orange) highlighted. (C) Homology model of EfpA with mutations conferring resistance to BRD-8000.3 (green) or BRD-9327 (orange) highlighted. Mesh outlines show possible binding sites of BRD-8000.3 (green) and BRD-9327 (orange), as determined by docking using AutoDock Vina. (D) Broth microdilution dose response assay of Mmar mutants resistant to BRD-8000.3 against BRD-9327, demonstrating the hypersensitivity of Mmar *efpA*(*V319M*) and Mmar *efpA*(*A415V*). Filled circles show the mean, and error bars indicate the 95% confidence interval (n = 4). (E) Loewe excess of Mmar growth inhibition at varying combined concentrations of BRD-9327 and BRD-8000.3, demonstrating potentiation of BRD-9327 by BRD-8000.3 between the two EfpA inhibitors.

Here, we demonstrate discovery acceleration afforded by PROSPECT and proof-of-concept for a novel strategy, which leverages chemical genetics in the design of compound combinations that inhibit the same target through different mechanisms. We show that BRD-9327 is indeed an uncompetitive inhibitor of EfpA, synergistic with BRD-8000, and mutations conferring high-level resistance to either of the two compounds, despite only arising in *efpA*, are mutually exclusive and can cause mutual collateral sensitivity to the other compound, thereby lowering the spontaneous resistance frequency to BRD-8000 in a BRD-9327-resistant background. Together, these observations point to a strategy in which the pair could be applied together in a resistance-suppressing combination or resistance cycling regimen. The discovery of BRD-9327 and its interaction with BRD-8000 demonstrates the power of large-scale chemical genetics as a primary screening modality, which predicts the MOA of active compounds. This enables the prioritization of active compounds to emphasize the MOA and the design of new strategies that rely on mechanistic knowledge instead of potency.

EfpA is an attractive antimycobacterial target since its inhibition was bactericidal and its activity is narrow spectrum (EfpA is only present in Actinomycetes); we therefore sought to expand the chemical lead space by identifying new chemotypes for EfpA inhibition. Our previous identification and validation of BRD-8000 and BRD-8000.3 as specific EfpA inhibitors[3] allowed us to leverage their CGIPs as references for EfpA inhibition. We identified new chemotypes that inhibit EfpA by prioritizing additional putative EfpA inhibitors from the original primary screening data based on their CGIP correlation with the CGIP of BRD-8000 (Figure 1C). This strategy yielded the identification of chemically distinct BRD-9327 as another possible EfpA inhibitor.[3] BRD-9327 showed very weak Mtb wild-type activity (>50 μM) but moderate activity against the EfpA hypomorph (6.25 μM, Figure 1D).

To determine if BRD-9327 is a specific inhibitor of the EfpA efflux pump in Mtb, we used an established ethidium bromide (EtBr) efflux assay to measure the impact of BRD-9327 on rates of efflux of EtBr, a substrate of EfpA.[4] EtBr is ∼30-fold more fluorescent when intracellular than when extracellular;[4] this property can be leveraged to measure the efflux-mediated decrease in intracellular EtBr concentration over time (Figure 2A). In the presence of varying inhibitor concentrations, we measured intracellular EtBr fluorescence over time at varying initial EtBr concentrations. We then globally fit a modified Michaelis–Menten equation (accounting for Fick diffusion as well as efflux) to the data, obtaining best-fit parameter estimates for the kinetic substrate-free inhibition constant (K_i) and substrate-bound inhibition constant (K_i')[5] (Figure 2B).

We measured EtBr efflux rates in *Mycobacterium smegmatis* MC^{2}155 (Msm), a related mycobacterial species, rather than Mtb directly, because Msm's growth is not affected by BRD-8000 or BRD-9327, presumably because its EfpA homologue (MSMEG_2619) is not essential.[6] We could thus remove the confounding effects of compounds on cellular viability to more cleanly study their direct effect on efflux. However, in addition to EfpA, Msm has a set of other nonessential multidrug efflux pumps that efflux EtBr. Thus, in order to determine the dependence of the efflux inhibition kinetic parameters on EfpA specifically (Figure 2A), we compared EtBr efflux in a Msm strain containing *efpA* and a strain in which *efpA* had been deleted (MsmΔ*efpA*).

In MsmΔ*efpA*, we found that BRD-9327 is a competitive inhibitor of EtBr efflux by the other multidrug efflux pumps, with a collective K_i/K_i' = 0.6 (Figure 2C; $K_i/K_i' < 1$ characterizes competitive inhibition). In contrast, BRD-9327 inhibited efflux in the presence of EfpA in wild-type Msm with

DOI: 10.1021/acsinfecdis.9b00373
ACS Infect. Dis. 2020, 6, 56−63

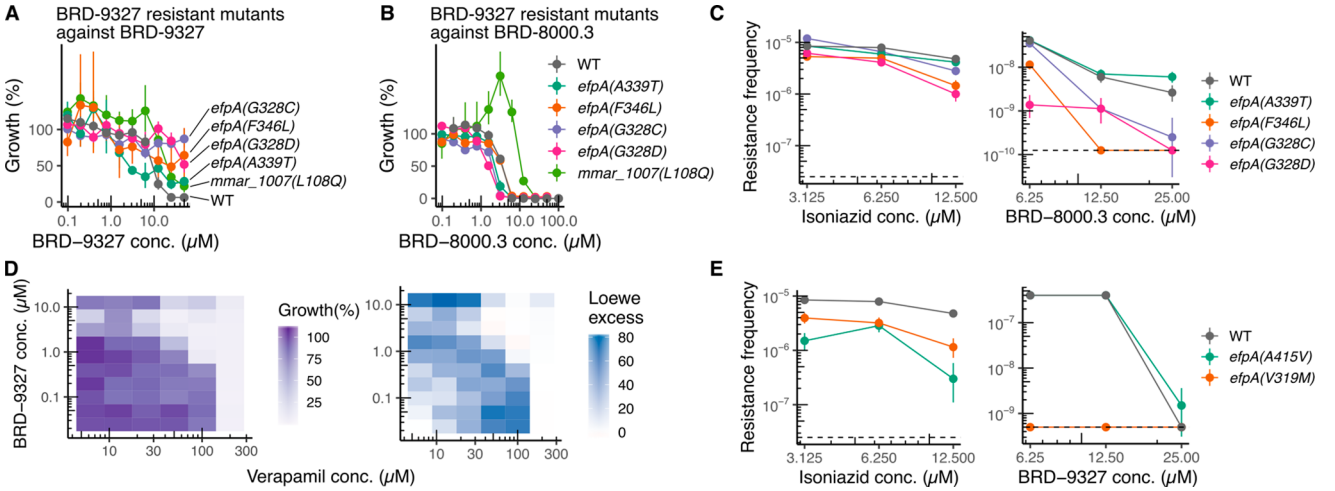

Figure 4. Resistance to BRD-9327 lowers the resistance frequency to BRD-8000.3. (A) Broth microdilution dose response assay of Mmar and its BRD-9327-resistant mutants against BRD-9327, demonstrating the high-level resistance of *efpA* mutants and low-level resistance of the *mmar_1007* mutant. Filled circles show the mean, and error bars indicate the 95% confidence interval (n = 4). (B) Broth microdilution dose response assay of Mmar mutants resistant to BRD-9327 against BRD-8000.3, demonstrating the hypersensitivity of Mmar *efpA*(*G328D*) and Mmar *efpA*(*A339T*). Filled circles show the mean, and error bars indicate the 95% confidence interval (n = 4). (C) Frequency of wild-type or BRD-9327-resistant mutant colonies growing on agar containing 2×, 4×, or 8× MIC of INH (left) or BRD-8000.3 (right). Filled circles show the mean, and error bars indicate the 95% confidence interval (n = 4). The dashed line indicates the limit of detection. (D) Growth inhibition from the broth microdilution assay of Mmar (left) and the Loewe excess (right) at varying combined concentrations of BRD-9327 and verapamil, demonstrating modest synergy between the two compounds. (E) Frequency of wild-type or BRD-8000.3 resistant mutant colonies growing on agar containing 2×, 4×, or 8× MIC of INH (left) or BRD-9327 supplemented with verapamil (right). Filled circles show the mean, and error bars indicate the 95% confidence interval (n = 4). The dashed line indicates the limit of detection.

a $K_i/K_i' = 5.3$ ($K_i/K_i' \geq 1$ characterizes non- or uncompetitive inhibition; Figure 2C). A mixed or uncompetitive inhibition modality in the presence of EfpA but competitive inhibition in its absence would suggest that, while BRD-9327 can be a general efflux substrate of the other efflux pumps, it is a specific, allosteric inhibitor of the EtBr efflux by EfpA. Complementation of MsmΔ*efpA* with the Mtb *efpA* homologue showed even more dramatic uncompetitive inhibition ($K_i/K_i' = 100$), compared to the wild-type Msm allele, and definitively demonstrated that BRD-9327 is an inhibitor of Mtb EfpA.

We had previously identified a single *efpA* allele in Mtb that confers resistance to BRD-8000 with the V319F amino acid substitution abolishing BRD-8000 binding to mutant EfpA.[3] Interestingly, when we complemented MsmΔ*efpA* with the *efpA*(*V319F*) allele, while competitive efflux inhibition is observed by BRD-8000.3 (due to its activity at the background multidrug efflux pumps in Msm), we observed uncompetitive efflux inhibition by BRD-9327 (Figure 2C). This uncompetitive inhibition of EfpA(V319F) revealed that BRD-9327 interacts with this mutant EfpA in a manner that must be distinct from the BRD-8000s interaction with EfpA. We therefore tested EtBr efflux inhibition by a combination of BRD-8000.3 and BRD-9327 and found these compounds to be synergistic by excess-over-Bliss (EoB)[7] (Figure S1A).

Having discovered that an allele of Mtb *efpA* that confers resistance to BRD-8000 does not confer biochemical cross-resistance to BRD-9327, we sought to determine if resistance to BRD-9327 would result in cross-resistance to BRD-8000. Because BRD-9327 had not been chemically optimized like the BRD-8000 series to have potent Mtb activity (Mtb MIC of BRD-9327 ≥ 50 μM), we turned to *Myobacterium marinum* M (Mmar), another related, pathogenic mycobacterial species, that was more sensitive to BRD-9327 (MIC = 25 μM, Figure 3D).

We first regenerated BRD-8000.3-resistant mutants in Mmar to provide a baseline comparison of BRD-8000 resistance conferring mutations in Mtb and Mmar. We plated exponentially growing bacteria on agar containing BRD-8000.3 at 2×, 4×, and 8× the broth microdilution MIC (6.25 μM in Mmar; Figure 3A) to obtain a resistance at a frequency of ∼4 × 10^{-8}, confirmed shifts in the broth microdilution MIC of selected colonies, and performed whole genome sequencing (WGS) of resistant clones on the Illumina MiSeq or HiSeq platform. Whereas we had only observed a single resistance-conferring variant in Mtb (V319F),[3] we isolated two different Mmar resistant mutants both containing alterations in Mmar *efpA*, V319M and A415V (Figure 3B), which conferred a >16-fold increase in MIC (Figure 3A). Although there is no high-resolution structure of EfpA, a homology model constructed with I-TASSER[8] suggested that Val_{319} and Ala_{415} are on neighboring α-helices and that these mutations could implement the same resistance mechanism (Figure 3C). Consistent with our finding that the *efpA*(*V319F*) allele of Mtb did not confer functional, biochemical cross-resistance to BRD-9327, BRD-8000.3 resistant mutants of Mmar did not have resistance to BRD-9327. In fact, surprisingly, Mmar *efpA*(*V319M*) was 4-fold more sensitive than the wild-type, with MIC of 6.25 μM for the mutant compared to 25 μM for wild-type Mmar (Figure 3D); although MIC of Mmar *efpA*(*A415V*) was >50 μM, it showed an IC_{50} of 800 nM. Interestingly, although both BRD-8000 resistant mutants' growth was inhibited by BRD-9327 concentrations below 25 μM, these strains showed unrestricted growth at BRD-9327 concentrations above 25 μM, possibly due to induction of other efflux pumps that extrude BRD-9327.

DOI: 10.1021/acsinfecdis.9b00373
ACS Infect. Dis. 2020, 6, 56−63

We next sought to identify Mmar *efpA* alleles that confer resistance to BRD-9327. While BRD-9327 is more potent against Mmar than Mtb, its corresponding MIC is nevertheless too high to allow straightforward selection. Instead, inspired by the efflux synergy of BRD-8000.3 with BRD-9327, we performed a checkerboard assay for growth inhibition of Mmar by the two compounds in combination (Figure S1B,C) and found that they were synergistic by Loewe additivity[9] (Figure 3E), EoB[7] (Figure S1D), and multidimensional synergy of combinations[10] (MuSyC; Figure S1E,F). In particular, BRD-8000.3 concentrations between 0.1 and 3 μM potentiated growth inhibition by BRD-9327. We therefore selected for mutants on agar containing 50 μM BRD-9327 supplemented with 3 μM BRD-8000.3. Since colonies that grew on this combination could escape selection pressure by evolving resistance to either compound, we picked and screened 21 colonies for resistance to each compound individually using a broth microdilution assay. WGS revealed *efpA* variants G328C, G328D, A339T, and F346L, which conferred high-level resistance to BRD-9327 but not BRD-8000.3 (Figure 3A). The same homology model of EfpA suggested that these mutated amino acids appeared to reside on neighboring α-helices, again indicating that they could implement the same resistance mechanism (Figure 3C). We identified an additional mutation resulting in a L108Q substitution in *mmar_1007*, the homologue of *Rv0678*, a transcriptional regulator of multidrug efflux pump MmpL5 in Mtb[11,12] (Figure S2A), which conferred low-level resistance to both BRD-9327 and BRD-8000.3 (Figure 4A,B), as well as clofazimine (Figure S2B), by increasing expression of MmpL5 and thus efflux of BRD-8000.3 and BRD-9327 (Figure S2C).

In parallel to the mutants resistant to BRD-8000 but hypersensitive to BRD-9327, the resistant mutants of BRD-9327 containing different *efpA* alleles did not exhibit cross-resistance to BRD-8000, and instead, some were hypersensitive to BRD-8000.3. The *efpA*(*G328C*), *efpA*(*G328D*), and *efpA*(*A339T*) mutants showed a 2-fold decrease in MIC for BRD-8000.3, while the other mutants with high-level BRD-9327 resistance were not resistant to BRD-8000.3 (Figure 4B). The unique interactions of the two EfpA inhibitors with EfpA, as revealed by their mutual collateral sensitivity, pointed to each having a narrow, target-specific resistance space, with mutations disrupting interactions with one compound exacerbating interactions to the other.

Given the mutual collateral sensitivity in the interaction of the two EfpA inhibitors, we speculated that these compounds could be used in a strategy to prevent the emergence of high-level resistance. To test this idea, we compared the resistance frequencies for BRD-8000.3 at 12.5, 25, and 50 μM in wild-type Mmar with the those in the Mmar mutants already resistant to BRD-9327. At 12.5 μM BRD-8000.3, while the resistance frequency of Mmar *efpA*(*F346L*) was 10^{-8}, a 4-fold decrease compared to wild-type Mmar, the resistance frequency of Mmar *efpA*(*G328D*) was 2×10^{-9}, a 20-fold decrease (Figure 4C). Whereas the wild-type resistance frequencies were 6×10^{-9} and 2×10^{-9} for 25 and 50 μM BRD-8000.3, no colonies could be recovered at all for *efpA*(*F346L*) on 25 μM BRD-8000.3 or higher nor for *efpA*(*G328D*) on 50 μM BRD-8000.3, indicating that BRD-9327 resistance lowers the probability of evolving BRD-8000 resistance (Figure 4C). The *efpA* mutant strains do not have an intrinsically higher mutation rate, as the resistance frequencies for isoniazid were identical (3×10^{-6}).

When we sought to perform the converse experiment to compare the resistance rates for BRD-9327 in wild-type Mmar with the rates in the BRD-8000 resistant Mmar $efpA_{V319F}$ mutant, using verapamil as a synergistic potentiator of BRD-9327 to lower its MIC to permit resistance selection in Mmar (Figures 4D and S3A–D), we again identified a barrier to resistance generation, now for evolving BRD-9327 resistance in a BRD-8000-resistant background. While wild-type Mmar showed unrestricted growth on 6.25 and 12.5 μM BRD-9327 in the presence of 3 μM verapamil and the resistance frequency for Mmar *efpA*(*A415V*) was comparable with wild-type Mmar ($\sim 10^{-9}$ at 25 μM), no BRD-9327-resistant mutants could be isolated at any concentration for Mmar *efpA*(*V319M*) (Figure 4E).

The power of large-scale chemical genetics as a primary screening modality, as implemented in PROSPECT, lies in its ability to incorporate putative MOA information into the prioritization of compounds, moving away from selection simply based on potency. After initial identification of an inhibitor of a new antimycobacterial target, EfpA, PROSPECT allowed for rapid target validation and iterative diversification of chemical scaffold space. With the identification of two chemically distinct EfpA inhibitors, BRD-8000 and BRD-9427, interestingly, we identified disjoint sets of target mutations conferring high-level resistance to the two scaffolds. Importantly, resistance to either compound mutually inflicts collateral sensitivity to the other, thereby raising the barrier against resistance to the combination.

The combination of BRD-8000.3 and BRD-9327 is a proof-of-principle demonstration of a novel strategy that leverages chemical genetics in the design of compound combinations restricting resistance space to a single essential gene, while inhibiting a single target by two different modalities in a manner that makes high-level resistance mutually exclusive. Their unique synergistic interaction illustrates the strategy for combining or cycling therapeutics, with the ability to increase the barriers to drug resistance even in the pursuit of a single target. The use of combination therapy is a critical characteristic of antimycobacterial drug regimens to tackle inevitable resistance evolution to any single agent, which has resulted in the current drug resistance crisis; the identification of rationally designed drug combinations or targets that manipulate the barrier to resistance evolution will be invaluable. This work identifies EfpA as one such valuable target because of its ability to be inhibited by BRD-8000 and BRD-9327 by mutually exclusive mechanisms. Whether EfpA is singularly unique, one of a small number of targets that are amenable to this strategy or represents a common theme to be more broadly exploited remains to be seen. Nevertheless, this work demonstrates that EfpA is an important and valuable target that can be exploited in this way. Importantly, the ability of PROSPECT to rapidly expand the diversity of scaffolds hitting a single target, as illustrated for EfpA, will enable the potential discovery of complementary inhibitors with variable mechanisms of action and facilitate greater exploration and expansion of this targeting strategy not only to tackle increasing tuberculosis drug resistance but also, more generally, to tackle other resistant pathogens and diseases such as cancer.

METHODS

Strains. The bacterial strains we used and designated as wild-type were *M. tuberculosis* H37Rv, *M. smegmatis* mc^2155,[13] and *M. marinum* M. Construction of the *M. smegmatis* Δ*efpA*

DOI: 10.1021/acsinfecdis.9b00373
ACS Infect. Dis. 2020, 6, 56–63

strain and expression constructs for *M. tuberculosis efpA* and *efpA*(*V319F*) were described previously.[3,14]

Compounds. BRD-8000 and BRD-8000.3 were synthesized and characterized as described previously.[3] BRD-9327 was purchased from ChemBridge (catalog #7025440).

Efflux Assay. Efflux rates were measured as previously described.[3] Briefly, Msm strains were grown in Middlebrook 7H9 medium (M7H9) supplemented with oleic acid, albumin, dextrose, and catalase (OADC; BD) to an OD_{600} of 0.4−0.6. Cultures were then centrifuged for 5 min at 3500 rpm. The pellet was washed once with phosphate buffered saline (PBS) at 37 °C and resuspended in 37 °C PBS to give a final OD_{600} of 0.4. Cultures were split into eight, and EtBr was added at a final concentration of 0.2−1.95 μg/mL; bacteria were incubated for 30 min (Msm) at 37 °C. After EtBr treatment, cells were centrifuged for 5 min at 3500 rpm and resuspended in 37 °C PBS to give a final OD_{600} of 0.8. A white 96-well plate (Corning) was prepared with serially diluted compound and 50 μL of PBS containing 0.8% w/v glucose. 50 μL of dye-loaded bacteria was added to each well of the plate. Fluorescence was read at 37 °C in a SpectraMax M5 plate reader using 530 nm excitation and 585 nm emission wavelengths for EtBr and was recorded every 30 s for 2 h (Msm).

To infer kinetic parameters, we modeled the rate of fluorescence decay as a modified Michaelis−Menten equation, which included a term for Fick diffusion[15] between the cytoplasm and extracellular mileu, as previously described.[3] Initial efflux rates to determine synergy were calculated by fitting a spline (function smooth.spline[16] in R) to each time course and calculating the first derivative at 480 s (to avoid knots in the spline).

Broth Microdilution Assays. The minimum inhibitory concentration of compounds was determined in a 96-well plate (Corning), filled with 49 μL of M7H9-OADC, and 1 μL of 100× compound DMSO stock. 50 μL of exponential-phase bacterial culture diluted to an OD_{600} of 0.005 was added. Plates were incubated at 37 °C in a humidified container for 3 d for Mmar and 14 d for Mtb. OD_{600} was measured using a SpectraMax M5 plate reader (Molecular Dimensions). Normalized percent outgrowth (NPO) was reported using

$$\mathrm{NPO} = (x_i - \mu_n)/(\mu_p - \mu_n) \tag{1}$$

where μ_p is the mean positive control value, μ_n is the mean negative control value, and x_i is the value of compound i.

Checkerboard Assays and Synergy. A 96-well plate (Corning) was filled with 48 μL of M7H9-OADC and 1 μL of each 100× compound DMSO stock. 50 μL of exponential-phase bacterial culture was diluted to an OD_{600} of 0.005 before being added. Synergy was calculated using three models: Loewe additivity,[9] excess-over-Bliss,[7] and multidimensional synergy of combinations (MuSyC).[10]

Loewe additivity[9] is a formalization of the dose additivity principle, which states that if two compounds do not interact then the observed effect of their combination will simply be the sum of their individual effects, adjusted for relative potency:

$$1 = [\mathrm{A}]/{f_\mathrm{A}}^{-1}(E_\mathrm{AB}) + [\mathrm{B}]/{f_\mathrm{B}}^{-1}(E_\mathrm{AB}) \tag{2}$$

where [A] and [B] are concentrations of compounds A and B combined to achieve effect E_{AB}; ${f_A}^{-1}$ and ${f_B}^{-1}$ are the inverse dose−response curves of compounds A and B (i.e., ${f_A}^{-1}(E_{AB})$ and ${f_B}^{-1}(E_{AB})$ are the concentrations of A and B required to achieve effect E_{AB}). To determine synergy, we first fit f_A and f_B as four-parameter Hill curves to the broth microdilution assays for compounds A and B. Then, we used the uniroot function in R to determine E_{AB} under the additivity model for each concentration of A and B in our checkerboard assay. We defined Loewe excess as the difference between the observed effect of the compound combination E_{AB} and the expected effect under the null additivity model.

Excess-over-Bliss[7] compares the expectation of independent compound effects to the observed combined effect:

$$E = E_\mathrm{AB} - (1 - (1 - f_\mathrm{A})(1 - f_\mathrm{B})) \tag{3}$$

where E is excess-over-Bliss, E_{AB} is the observed, combined fractional inhibition by the two compounds, and f_A and f_B are the observed individual fractional inhibition by each compound. The Z-score of EoB was calculated as E/s_E, where s_E is the estimated standard deviation of the EoB, calculated by propagating the standard deviations of the underlying growth or efflux rate measurements; the conventional Z-score cutoff of 3 was defined as significantly synergistic.

MuSyC[10] models compound interactions as a two-dimensional Hill surface:

$$\begin{aligned} E_\mathrm{AB} = {} & ({K_\mathrm{A}}^{h\mathrm{A}}{K_\mathrm{B}}^{h\mathrm{B}}E_0 + [\mathrm{A}]^{h\mathrm{A}}{K_\mathrm{B}}^{h\mathrm{B}}M_\mathrm{A} + {K_\mathrm{A}}^{h\mathrm{A}}[B]^{h\mathrm{A}}M_\mathrm{B} \\ & + (\alpha[A])^{h\mathrm{A}}[B]^{h\mathrm{B}}M_\mathrm{AB})/({K_\mathrm{A}}^{h\mathrm{A}}{K_\mathrm{B}}^{h\mathrm{B}} + [\mathrm{A}]^{h\mathrm{A}}{K_\mathrm{B}}^{h\mathrm{B}} + {K_\mathrm{A}}^{h\mathrm{A}}[B]^{h\mathrm{A}} \\ & + (\alpha[A])^{h\mathrm{A}}[B]^{h\mathrm{B}}) \end{aligned} \tag{4}$$

where [A] and [B] are concentrations of compounds A and B combined to achieve effect E_{AB}, K_A and K_B are the IC_{50} (potency) values of compounds A and B, hA and hB are the Hill constants of compounds A and B, E_0 is the growth in the absence of either compound, M_A and M_B are the maximal effects (efficacy) of compounds A and B alone, M_{AB} is the maximal effect of A and B combined, and α is the mutually potentiating effect between A and B. A and B are synergistic in potency if $\alpha > 1$ and antagonistic in potency otherwise. Synergy in efficacy is defined as $\beta = (\min(M_A, M_B) - M_{AB})/(E_0 - \min(M_A, M_B))$; A and B are synergistic in efficacy if $\beta > 0$ and antagonistic in efficacy otherwise. We determined the parameters K_A, K_B, hA, hB, E_0, M_A, M_B, M_{AB}, and α using nonlinear least-squares, as implemented in the nls function in R, to globally fit the MuSyC model to our checkerboard data.

Evolution of Resistant Mutants. Midexponential growth-phase bacterial cultures were pelleted and resuspended at 2×10^{10} cfu mL^{-1} in M7H9-OADC. 50 μL (10^9 cfu) was plated in duplicate on 6 mL of M7H10-OADC agar containing 2×, 4×, or 8× MIC of the test compound. Plates were incubated at 37 °C in a humidified container. This was repeated on two separate days. At 14 d, agar was checked every 7 d for colonies, which were transferred to 10 mL of M7H9-OADC, and cultures were grown to midexponential phase before testing for resistance in a broth microdilution assay. Resistant mutants were then subjected to whole genome sequencing.

Whole Genome Sequencing of Mycobacteria. Ten μL of bacterial culture was combined with 10 μL of 10% v/v DMSO in a 96-well clear round-bottom plate (Corning). Plates were heat-inactivated at 80 °C for 2 h. Genomic DNA (gDNA) was separated from intact cells and cell debris using AMPure XP (Beckman), eluting in 40 μL of Milli-Q water. 1.5 μL of gDNA was amplified using 6 μM random primers (Invitrogen) and φ29 DNA Polymerase (NEB) in a 10 μL reaction volume at 30 °C for 24 h.

DOI: 10.1021/acsinfecdis.9b00373
ACS Infect. Dis. 2020, 6, 56−63

Amplified gDNA was purified using AMPure XP and subjected to NextEra XT NGS library construction (Illumina) before 150-cycle paired-end sequencing on the Illumina MiSeq platform. Reads were aligned to the CP000854 reference sequence[17] using the BWA-mem[18] algorithm, and mutations were called using the Genome Analysis Toolkit (GATK).[19]

Computational Modeling of Proteins and Ligands. A homology model of EfpA was built using the I-TASSER algorithm,[8] which builds a model from an ensemble of templates, each of which has some sequence homology to a region of the query. For the essential efflux pump, EfpA, I-TASSER used peptide and oligopeptide transporters (PDB 4IKV,[20] 4Q65,[21] 4W6V,[22] 6EI3,[23] 6GS1[24]), human glucose transporter GLUT1 (4PYP[25]), *E. coli* multidrug transporter MdfA[26] (4ZOW), and *E. coli* organic ion transporter DgoT (6E9N[27]) as templates.

Possible binding sites of BRD-8000.3 and BRD-9327 in the I-TASSER model were calculated using the AutoDock Vina[28] extension of UCSF Chimera.[29]

■ ASSOCIATED CONTENT

Supporting Information

The Supporting Information is available free of charge on the ACS Publications website at DOI: 10.1021/acsinfecdis.9b00373.

Synergy between BRD-8000.3 and BRD-9327, regulation of MmpL5 by *mmar_1005*, and synergy between verapamil and BRD-9327 (PDF)

■ AUTHOR INFORMATION

Corresponding Author

*E-mail: hung@broadinstitute.org.

ORCID

Eachan O. Johnson: 0000-0002-0335-8337

Deborah T. Hung: 0000-0003-4262-0673

Author Contributions

The project was devised by E.O.J. and D.T.H. Experiments were designed by E.O.J. Experiments were carried out and results were analyzed by E.O.J. and E.O. Compounds were synthesized by T.K. Homology modeling and docking were carried out by E.O.J. and M.O. E.O.J. and D.T.H. wrote the manuscript.

Notes

The authors declare no competing financial interest.

■ ACKNOWLEDGMENTS

Funding was provided by the Broad Institute TB Gift Donors, Pershing Square Foundation, and the Bill and Melinda Gates Foundation.

■ ABBREVIATIONS

Mtb, *Mycobacterium tuberculosis*; Mmar, *Mycobacterium marinum*; Msm, *Mycobacterium smegmatis*; MIC, minimum inhibitory concentration; DMSO, dimethyl sulfoxide; OADC, oleic acid, albumin, dextrose, and catalase; OD_{600}, optical density at 600 nm

■ REFERENCES

(1) W.H.O. (2019) *Global Tuberculosis Report 2019*, World Health Organization, Geneva.

(2) Conradie, F., Diacon, A. H., Everitt, D., Mendel, C., van Niekerk, C., Howell, P., Comins, K., and Spigelman, M. (2017) The Nix-TB Trial of Pretomanid, Bedaquiline and Linezolid to Treat XDR-TB. In *Conference on Retroviruses and Opportunistic Infections*, Seattle, WA.

(3) Johnson, E. O., LaVerriere, E., Office, E., Stanley, M., Meyer, E., Kawate, T., Gomez, J. E., Audette, R. E., Bandyopadhyay, N., Betancourt, N., Delano, K., Da Silva, I., Davis, J., Gallo, C., Gardner, M., Golas, A. J., Guinn, K. M., Kennedy, S., Korn, R., McConnell, J. A., Moss, C. E., Murphy, K. C., Nietupski, R. M., Papavinasasundaram, K. G., Pinkham, J. T., Pino, P. A., Proulx, M. K., Ruecker, N., Song, N., Thompson, M., Trujillo, C., Wakabayashi, S., Wallach, J. B., Watson, C., Ioerger, T. R., Lander, E. S., Hubbard, B. K., Serrano-Wu, M. H., Ehrt, S., Fitzgerald, M., Rubin, E. J., Sassetti, C. M., Schnappinger, D., and Hung, D. T. (2019) Large-scale chemical–genetics yields new M. tuberculosis inhibitor classes. *Nature 571*, 72–78.

(4) Paixao, L., Rodrigues, L., Couto, I., Martins, M., Fernandes, P., de Carvalho, C. C., Monteiro, G. A., Sansonetty, F., Amaral, L., and Viveiros, M. (2009) Fluorometric determination of ethidium bromide efflux kinetics in *Escherichia coli*. *J. Biol. Eng. 3*, 18.

(5) Strelow, J., Dewe, W., Iversen, P. W., Brooks, H. B., Radding, J. A., McGee, J., and Weidner, J. (2004) Mechanism of Action Assays for Enzymes. In *Assay Guidance Manual*, Eli Lilly & Company and the National Center for Advancing Translational Sciences, Bethesda, MD.

(6) Li, X. Z., Zhang, L., and Nikaido, H. (2004) Efflux pump-mediated intrinsic drug resistance in Mycobacterium smegmatis. *Antimicrob. Agents Chemother. 48*, 2415–2423.

(7) Bliss, C. I. (1939) The Toxicity of Poisons Applied Jointly. *Ann. Appl. Biol. 26*, 585–615.

(8) Yang, J., Yan, R., Roy, A., Xu, D., Poisson, J., and Zhang, Y. (2015) The I-TASSER Suite: protein structure and function prediction. *Nat. Methods 12*, 7–8.

(9) Loewe, S., and Muischnek, H. (1926) Über Kombinationswirkungen. *Naunyn-Schmiedeberg's Arch. Pharmacol. 114*, 313–326.

(10) Meyer, C. T., Wooten, D. J., Paudel, B. B., Bauer, J., Hardeman, K. N., Westover, D., Lovly, C. M., Harris, L. A., Tyson, D. R., and Quaranta, V. (2019) Quantifying Drug Combination Synergy along Potency and Efficacy Axes. *Cell Syst. 8*, 97–627834880.

(11) Andries, K., Villellas, C., Coeck, N., Thys, K., Gevers, T., Vranckx, L., Lounis, N., de Jong, B. C., and Koul, A. (2014) Acquired resistance of Mycobacterium tuberculosis to bedaquiline. *PLoS One 9*, No. e102135.

(12) Hartkoorn, R. C., Uplekar, S., and Cole, S. T. (2014) Cross-Resistance between Clofazimine and Bedaquiline through Upregulation of MmpL5 in Mycobacterium tuberculosis. *Antimicrob. Agents Chemother. 58*, 2979–2981.

(13) Snapper, S. B., Melton, R. E., Mustafa, S., Kieser, T., and Jacobs, W. R., Jr. (1990) Isolation and characterization of efficient plasmid transformation mutants of Mycobacterium smegmatis. *Mol. Microbiol. 4*, 1911–1919.

(14) Murphy, K. C., Nelson, S. J., Nambi, S., Papavinasasundaram, K., Baer, C. E., and Sassetti, C. M. (2018) ORBIT: a New Paradigm for Genetic Engineering of Mycobacterial Chromosomes. *mBio 9*, e01467–01418.

(15) Fick, A. (1855) Ueber Diffusion. *Ann. Phys. (Berlin, Ger.) 170*, 59–86.

(16) Chambers, J. M., and Hastie, T. J. (1992) *Statistical Models in S*, Wadsworth & Brooks/Cole.

(17) Stinear, T. P., Seemann, T., Harrison, P. F., Jenkin, G. A., Davies, J. K., Johnson, P., Abdellah, Z., Arrowsmith, C., Chillingworth, T., Churcher, C., Clarke, K., Cronin, A., Davis, P., Goodhead, I., Holroyd, N., Jagels, K., Lord, A., Moule, S., Mungall, K., Norbertczak, H., Quail, M. A., Rabbinowitsch, E., Walker, D., White, B., Whitehead, S., Small, P., Brosch, R., Ramakrishnan, L., Fischbach, M. A., Parkhill, J., and Cole, S. T. (2008) Insights from the complete genome sequence of Mycobacterium marinum on the evolution of Mycobacterium tuberculosis. *Genome Res. 18*, 729–741.

DOI: 10.1021/acsinfecdis.9b00373
ACS Infect. Dis. 2020, 6, 56–63

(18) Li, H., and Durbin, R. (2009) Fast and accurate short read alignment with Burrows−Wheeler transform. *Bioinformatics 25*, 1754−1760.
(19) Van der Auwera, G. A., Carneiro, M. O., Hartl, C., Poplin, R., Del Angel, G., Levy-Moonshine, A., Jordan, T., Shakir, K., Roazen, D., Thibault, J., Banks, E., Garimella, K. V., Altshuler, D., Gabriel, S., and DePristo, M. A. (2013) From FastQ data to high confidence variant calls: the Genome Analysis Toolkit best practices pipeline. *Curr. Protoc. Bioinf. 43*, 11.10.1−11.10.33.
(20) Doki, S., Kato, H. E., Solcan, N., Iwaki, M., Koyama, M., Hattori, M., Iwase, N., Tsukazaki, T., Sugita, Y., Kandori, H., Newstead, S., Ishitani, R., and Nureki, O. (2013) Structural basis for dynamic mechanism of proton-coupled symport by the peptide transporter POT. *Proc. Natl. Acad. Sci. U. S. A. 110*, 11343−11348.
(21) Zhao, Y., Mao, G., Liu, M., Zhang, L., Wang, X., and Zhang, X. C. (2014) Crystal Structure of the E. coli Peptide Transporter YbgH. *Structure 22*, 1152−1160.
(22) Boggavarapu, R., Jeckelmann, J. M., Harder, D., Ucurum, Z., and Fotiadis, D. (2015) Role of electrostatic interactions for ligand recognition and specificity of peptide transporters. *BMC Biol. 13*, 58.
(23) Parker, J. L., Li, C., Brinth, A., Wang, Z., Vogeley, L., Solcan, N., Ledderboge-Vucinic, G., Swanson, J. M. J., Caffrey, M., Voth, G. A., and Newstead, S. (2017) Proton movement and coupling in the POT family of peptide transporters. *Proc. Natl. Acad. Sci. U. S. A. 114*, 13182−13187.
(24) Ural-Blimke, Y., Flayhan, A., Strauss, J., Rantos, V., Bartels, K., Nielsen, R., Pardon, E., Steyaert, J., Kosinski, J., Quistgaard, E. M., and Löw, C. (2019) Structure of Prototypic Peptide Transporter DtpA from E. coli in Complex with Valganciclovir Provides Insights into Drug Binding of Human PepT1. *J. Am. Chem. Soc. 141*, 2404−2412.
(25) Deng, D., Xu, C., Sun, P., Wu, J., Yan, C., Hu, M., and Yan, N. (2014) Crystal structure of the human glucose transporter GLUT1. *Nature 510*, 121.
(26) Heng, J., Zhao, Y., Liu, M., Liu, Y., Fan, J., Wang, X., Zhao, Y., and Zhang, X. C. (2015) Substrate-bound structure of the E. coli multidrug resistance transporter MdfA. *Cell Res. 25*, 1060.
(27) Leano, J. B., Batarni, S., Eriksen, J., Juge, N., Pak, J. E., Kimura-Someya, T., Robles-Colmenares, Y., Moriyama, Y., Stroud, R. M., and Edwards, R. H. (2019) Structures suggest a mechanism for energy coupling by a family of organic anion transporters. *PLoS Biol. 17*, e3000260.
(28) Trott, O., and Olson, A. J. (2010) AutoDock Vina: Improving the speed and accuracy of docking with a new scoring function, efficient optimization, and multithreading. *J. Comput. Chem. 31*, 455−461.
(29) Pettersen, E. F., Goddard, T. D., Huang, C. C., Couch, G. S., Greenblatt, D. M., Meng, E. C., and Ferrin, T. E. (2004) UCSF Chimera—A visualization system for exploratory research and analysis. *J. Comput. Chem. 25*, 1605−1612.

DOI: 10.1021/acsinfecdis.9b00373
ACS Infect. Dis. 2020, 6, 56−63